A novel micronemal protein, Scot1, is essential for apicoplast biogenesis and liver stage development in *Plasmodium berghei*

Ankit Ghosh[1], Akancha Mishra[1,2], Raksha Devi[1,2], Sunil Kumar Narwal[1], Nirdosh[1,2], Pratik Narain Srivastava[1], Satish Mishra[1,2*]

[1]Division of Molecular Microbiology and Immunology, CSIR-Central Drug Research Institute, Lucknow 226031, India.

[2]Academy of Scientific and Innovative Research (AcSIR), Ghaziabad 201002, India.

Corresponding author: Satish Mishra

Email: satish.mishra@cdri.res.in

ORCID ID:

Satish Mishra: 0000-0002-8942-6416

Ankit Ghosh: 0009-0005-5615-1208

Akancha Mishra: 0009-0005-4775-3338

Raksha Devi: 0009-0009-6929-766X

Sunil Kumar Narwal: 0000-0001-5476-9753

Nirdosh: 0009-0005-9930-3865

Pratik Narain Srivastava: 0000-0001-9273-675X.

Running title: Scot1 regulates parasite maturation in the liver.

Abstract

Plasmodium sporozoites invade hepatocytes, transform into liver stages, and replicate into thousands of merozoites that infect erythrocytes and cause malaria. Proteins secreted from micronemes play an essential role in hepatocyte invasion, and unneeded micronemes are subsequently discarded for replication. The liver-stage parasites are potent immunogens that prevent malarial infection. Late liver stage-arresting genetically attenuated parasites (GAPs) exhibit greater protective efficacy than early GAP. However, the number of late liver-stage GAPs for generating GAPs with multiple gene deletions is limited. Here, we identified Scot1 (Sporozoite Conserved Orthologous Transcript 1), which was previously shown to be upregulated in sporozoites, and by endogenous tagging with mCherry, we demonstrated that it is expressed in the sporozoite and liver stages in micronemes. Using targeted gene deletion in *Plasmodium berghei*, we showed that Scot1 is essential for late liver-stage development. *Scot1* KO sporozoites grew normally into liver stages but failed to initiate blood-stage infection in mice due to impaired apicoplast biogenesis and merozoite formation. Bioinformatic studies suggested that Scot1 is a metal/small molecule carrier protein. Remarkably, supplementation with metals in the culture of infected *Scot1* KO cells did not rescue their phenotype. Immunization with *Scot1* KO sporozoites in C57BL/6 mice confers protection against a malaria challenge via infection. These proof-of-concept studies will enable the generation of *P. falciparum Scot1* mutants that could be exploited to generate GAP malaria vaccines.

Importance

Malaria parasites experience significant bottlenecks as transmitted to the mammalian host during a mosquito bite. Sporozoites invade liver cells, reproducing into thousands of merozoites, which are released after liver cell ruptures. The specific arrest of sporozoites during liver stage development acts as a powerful immunogen and provides sterile protection against sporozoite infection. GAP leading to an arrest in late liver stage development offers superior protection. Here, we report that a micronemal protein, Scot1, is essential for parasite maturation in the liver. Deletion of Scot1 resulted in impaired apicoplast biogenesis and merozoite formation. Vaccination with *Scot1* KO sporozoites protects against malaria challenge. We have identified a late arresting GAP that will aid in developing new as well as safeguarding existing whole parasite vaccines.

Keywords: GAP; *Plasmodium*; microneme; liver stage; malaria; preerythrocytic; protection; sporozoite; vaccine.

Introduction

Malaria has a tremendous negative impact on human health and the economy, a trend that unfortunately continues even today. Malaria-causing *Plasmodium* parasites are responsible for more than 249 million cases and 0.61 million deaths in 2022 (1). *Plasmodium* sporozoites are transmitted via the bite of an infected *Anopheles* mosquito, which invades the liver and transforms into exoerythrocytic forms (EEFs). Within hepatocytes, the parasite undergoes intracellular replication and forms thousands of merozoites, which initiate pathogenic erythrocytic stages (2). The parasite must eliminate unnecessary micronemes throughout this development process to create room for newly synthesized stage-specific organelles and proteins (3). It was recently demonstrated that the *Plasmodium* autophagy pathway is essential for eliminating unneeded micronemes during the development of the parasite liver stages (4). However, the contributions of micronemal resident proteins to eliminating micronemes remain unknown. To date, micronemal proteins are secreted during invasion and play a crucial role in the gliding motility and infectivity of *Plasmodium* sporozoites (5).

The micronemal protein TRAP (Thrombospondin-related anonymous protein) links the sporozoite actin/myosin motor to the extracellular substrate and was shown to be essential for gliding motility (5, 6). Other micronemal proteins, such as SPECT (sporozoite microneme protein essential for cell traversal), MAEBL (merozoite apical erythrocyte-binding ligand), P36, P52, GAMA (GPI-anchored micronemal antigen), CelTOS (cell traversal for ookinetes and sporozoites), TRP1 (Thrombospondin-related protein 1), S6/TREP and AMA1 (Apical Membrane Antigen 1), have been characterized in *Plasmodium* (5). CelTOS, MAEBL, SPECT, and AMA1 are involved

in cell traversal (5, 7). In addition to erythrocyte invasion, AMA1 was shown to be secreted from sporozoites and drive their invasion (5, 8). S6/TREP was found to be important for parasite motility and efficient malaria transmission (9). P36 and P52 form a complex and play an essential role in the productive invasion of sporozoites (5). Disruption of P52 and P36 leads to the attenuation of parasites in the liver and confers sterile immunity against infection (10). GAMA and TRP1 were found to be important for sporozoite egress from oocysts (11, 12).

The emergence and spread of artemisinin-resistant *P. falciparum* threatens the control and elimination of malaria. New drugs and a highly effective malaria vaccine are urgently needed. The World Health Organization (WHO) has recommended using the circumsporozoite protein (CSP)-based RTS,S vaccine despite its modest efficacy (13). R21/Matrix-M is the second malaria vaccine recommended by the WHO (14). The major drawback of this recombinant vaccine is the lack of an efficient and durable immune response, which may not be suitable for long-term usage. Occasionally, subunit vaccines do not elicit as strong or long-lasting immune response as whole-organism vaccines. The radiation-attenuated sporozoite (RAS) vaccine has existed for several decades and has been proven to have long-term protective effects (15). Moreover, the induction of sterile immunity by the RAS was very encouraging. Nonetheless, one of the main drawbacks of this approach is that either underirradiation leads to breakthrough infection, or overirradiation of sporozoites leads to failure in initiating optimal preerythrocytic immunity (16). Immunization with live sporozoites attenuated by genetic modification has attracted much attention because they have been shown to produce protective immune responses equal to or even greater than those produced by irradiated sporozoites in

rodent models (17). The protection of these attenuated sporozoite vaccines involves antibodies elicited against sporozoite antigens that neutralize their ability to invade hepatocytes (18). Moreover, this protection is mediated through CD8+ T-cell responses that target infected hepatocytes (19).

The *P. falciparum* RAS vaccine expresses thousands of proteins and elicits superior protection compared to RTS,S; however, it does not confer complete protection in endemic areas (20) and requires improvement. Recent advances in *Plasmodium* genetics have enabled the generation of many GAPs, which have overcome the limitations of using RAS as a whole-organism vaccine. However, except for a few GAPs, most of these GAPs are blocked at the early to mid-liver stage, which limits the antigen breadth and biomass for superior immune protection (21). It was shown that immunization with *P. falciparum* sporozoites under a drug cover allows liver-stage parasites to mature, generating durable protection at lower doses than the *P. falciparum* RAS sporozoite vaccine (22). Although arrested parasites are a source of antigen for effective immune system priming, their antigenic repertoire induces cross-stage immunity only when parasites are blocked at the late liver stage (23). Since late liver stages exhibit a subset of antigens common to blood stages, identifying sporozoite genes that can yield a late arrest mutant will have a broader impact on developing an efficacious GAP vaccine. Here, we disrupted the function of the *P. berghei* micronemal protein Scot1 and investigated its role during late liver stage development. Immunization with late arresting GAP confers protection against infectious sporozoites.

Results

Scot1 is a highly conserved *Plasmodium*-specific protein

Phylogenetic analysis revealed that Scot1 is a *Plasmodium*-specific protein that is absent in other organisms (Figure S1). Scot1 was found to be highly conserved among *Plasmodium* species (Figure S2A). The identity matrix showed 100% sequence similarity between *P. berghei*, *P. yoelii* and *P.vinckei* and 92.1% similarity between *P. berghei* and *P. falciparum* and 90.9% similarity with *P. knowlesi* (Figure S2B). The Scot1 protein lacks a signal sequence and transmembrane domain.

Scot1 is expressed during the sporozoite and liver stages and is localized to the microneme

To study the expression and localization of Scot1, the gene was endogenously tagged with 3XHA-mCherry using double crossover homologous recombination (Figure S3A). Correct integration of the *Scot1* gene was confirmed by diagnostic PCR (Figure S3B). The development of transgenic parasites was analysed in mosquito and mammalian hosts. We found that the C-terminal tag did not affect parasite development throughout the life cycle (Figure S3C and S3D). The Scot1 promoter expressed the Scot1-mCherry protein in oocyst and salivary gland sporozoites and liver stages at 12, 24, and 62 hpi (Figure 1A, B and S3E). mCherry expression was not detected in the blood, gamete, ookinete, or liver stages at 36 or 48 hpi. The expression of the Scot1-3XHA-mCherry fusion protein was also confirmed by immunoblotting using an anti-mCherry antibody (Figure 1C). We then analysed the localization of Scot1-3XHA-mCherry in sporozoites and liver stages. Sporozoites were stained with anti-mCherry and anti-TRAP antibodies. We observed a granular localization pattern of Scot1-3XHA-mCherry, which colocalized with the TRAP signal in sporozoites, indicating that Scot1 is a micronemal protein (Figure

1D). These results indicate that Scot1 is expressed in sporozoites and liver stages and is localized to the microneme.

Scot1 is dispensable in the *P. berghei* blood and mosquito stages

To investigate the role of Scot1 in the parasite life cycle, we disrupted the gene in *P. berghei* using double crossover homologous recombination (Figure S4A). Resistant GFP (green fluorescent protein)-expressing parasites were confirmed by fluorescence microscopy (Figure S4B), and correct genomic integration was confirmed by diagnostic PCR (Figure S4C). A Scot1-complemented parasite line was generated by transfecting the *Scot1* expression cassette into *Scot1* KO schizonts (Figure S4D). Restoration of the *Scot1* locus was confirmed by diagnostic PCR (Figure S4E). To determine whether the deletion of *Scot*1 affected the dynamics of blood growth, two groups of mice were intravenously inoculated with WT GFP and *Scot1* KO parasites. Parasite growth was monitored by making Giemsa-stained blood smears. No difference was observed between WT GFP and *Scot1* KO parasites (Figure S4F). For the phenotypic characterization of the *Scot1* KO parasites, the mosquito cycle was initiated by infecting *A. stephensi* mosquitos with *Scot1* KO or WT GFP parasites. On day 14 postinfection, the mosquito midgut was dissected to check for the presence of oocysts, which was comparable in both WT GFP and *Scot1* KO parasites (Figure S5A and B). The sporogony in oocyst and sporozoite numbers were also normal (Figure S5C and D). Furthermore, on days 18-22 after a blood meal, the salivary glands were observed under a fluorescence microscope, and the sporozoite numbers were counted, which revealed a normal sporozoite load and number (Figure S5E and F). These results demonstrate that the

deletion of *Scot*1 does not affect parasite development in the blood or mosquito stages.

***Scot1* KO sporozoites infect the liver but fail to initiate blood-stage infection in mice**

To assess the in vivo infectivity of the *Scot1* KO parasites, salivary gland sporozoites were injected intravenously into C57BL/6 mice or infected by mosquito bites, and the appearance of the parasites in the blood was monitored by making Giemsa-stained blood smears. The WT GFP-inoculated mice were positive on day 3 post infection, whereas *Scot1* KO sporozoites failed to initiate blood-stage infection (Table 1). Scot1 gene complementation restored the KO phenotype (Table 1), indicating the specificity of the gene function. Micronemal proteins were previously shown to be required for the invasion of hepatocytes (24, 25). Therefore, we checked the invasion ability of the *Scot*1 KO sporozoites and found that they were normal (Figure S6). To analyse the progression of the parasites in vivo, the livers of infected mice were harvested at 40 and 55 hpi, and the parasite burden was quantified by amplifying 18S rRNA using real-time PCR. We found no difference in the 18S rRNA copy number at 40 hpi, but it was significantly lower at 55 hpi in the *Scot1* KO parasites than in the WT GFP parasites (Figure 2). These results provide evidence that *Scot1* KO parasites grow normally until the mid- to late-liver stage but do not mature and fail to initiate blood-stage infection in mice.

***Scot1* KO EEFs grow normally in size**

The normal invasion and failure of *Scot1* KO sporozoites to initiate blood-stage infection in mice suggest that either they failed to develop into EEFs or egress from hepatocytes. To further investigate the liver stage development of the *Scot1* KO parasites, HepG2 cells were infected with sporozoites and fixed at different time points. The liver stages of the WT GFP and *Scot1* KO parasites showed similar growth, EEF numbers, and sizes (Figure 3A-C). *Scot1* KO EEF growth, number, and size analysis revealed no apparent aberrant phenotype; however, there was evidence of reduced nuclear division at 62 hpi. Next, we observed the culture for the formation of detached cells at 62 hpi. We found detached cells in the WT GFP culture but not in the *Scot1* KO-infected culture (Figure 3D). Next, we checked the infectivity of detached cells from WT GFP and culture supernatant from *Scot1* KO parasites in Swiss mice. We found infection in mice injected with WT GFP-detached cells; no infection was observed in the KO-injected group (Table 2).

Scot1 KO parasites exhibit impaired apicoplast biogenesis and fail to mature into hepatic merozoites

Next, we analysed late liver-stage parasites by immunostaining with ACP (Acyl Carrier Protein) and MSP1 (Merozoite Surface Protein 1) antibodies. Loss of *Scot1* severely compromised apicoplast biogenesis, resulting in a consequent loss of MSP1 staining and no merozoite formation (Figure 4A and B). We found impaired nuclear division and a significant decrease in the number of nuclei in the *Scot1* KO parasites compared to those in the WT GFP parasites (Figure 4C). These results indicated the role of Scot1 during late liver-stage development.

Scot1 is not required for the elimination of micronemes

After sporozoite invasion, unneeded micronemes are expelled into the PV during liver stage development (3, 26). To determine whether the microneme-localized protein Scot1 is involved in eliminating micronemes, we monitored its distribution pattern during liver stage development using an anti-TRAP antibody. We found that by 24 hpi, the micronemes were directed toward the PV membrane of the parasite, and by 40-55 hpi, all the micronemes were expelled into the PV membrane, indicating normal elimination of the micronemes from the *Scot1* KO and WT GFP parasites (Figure 5). These data indicate that Scot1 is dispensable for the elimination of micronemes.

Bioinformatic studies suggest that Scot1 is a metal/small molecule carrier protein

Structural modelling of PfScot1 revealed a beta-pleated sheet structure twisted in itself, forming an open barrel shape (Figure 6A). Structural superposition with the SCOP and PDB databases using the FATCAT and DALI web services and subsequent superposition of the results in UCSF Chimera showed that the model aligns with the haemoglobin linker chain L1 (chain M of PDB ID 2GTL (red)) with a 0.9 Angstrom RMSD value (Figure 6B) and chain A of the crystal structure of the vaccine antigen Transferrin Binding Protein B (TbpB) (PDB ID: 4O4X (red)), a metal transport protein with a 0.8 Angstrom RMSD value (Figure 6C). The top hits from the structure-based phylogenetic analysis further emphasize the possible function of PfScot1 as a carrier of metal ions or small molecules (Figure 6D). Proteins with the closest structural similarity to that of Scot1 are listed in Table S1. A protein of unknown function from *Bacteroides eggerthii* DSM 20697 with a lipocalin-like domain was revealed to be most phylogenetically similar to Scot1. One of the most common

functions of the lipocalin-like domain is the transport of small molecules. An *E. coli* protein, YodA, with a lipocalin-like architecture is also known to bind metal ions to its barrel core. These results support the predicted structure-based annotation of Scot1 as a possible metal/small molecule carrier protein.

The *Scot1* KO phenotype is not reversed by iron, zinc or cadmium

To determine whether Scot1 is a carrier of metal ions and whether supplementation with metals can rescue the KO phenotype. WT GFP and *Scot1* KO liver-stage cultures were grown in media supplemented with 50 µg /ml ferric ammonium citrate (FAC), 20 µM zinc chloride (ZnCl2) or 1µg/ml cadmium chloride (CdCl2). We observed the culture for the formation of detached cells at 65 hpi. We found detached cells in the WT GFP culture but not in the *Scot1* KO infected culture supplemented with metal ions (Figure 7A). Next, we checked the infectivity of detached cells from WT GFP and culture supernatant from *Scot1* KO parasites in Swiss mice. We found that culture treatment with metal ions did not affect detached cell formation or infection in mice (Table 3). This treatment also did not affect the maturation of EEFs or nuclear division (Figure 7B, and C). These data show that Scot1 is not a carrier of iron, zinc, or cadmium and can possibly act as a carrier for other small molecules. Another possibility is that Scot1 may detoxify metal/small molecules. However, this requires further investigation.

Immunization with *Scot1* KO sporozoites protects against malaria

Immunizations with sporozoites that arrest in the liver elicit a long-term protective host response and protect against infectious sporozoite challenge (27). We tested whether immunization with *Scot1* KO sporozoites confers protection from WT

sporozoite infection. We observed that while all salivary gland debris-immunized mice developed blood-stage infection, the *Scot1* KO-immunized mice remained negative for the duration of the experiment (Table 4). These results are especially impressive since immunization of C57BL/6 mice with irradiated sporozoites rarely results in the immunity observed with *Scot1* KO sporozoites (28). Preerythrocytic protection after sporozoite immunization has revealed the induction of antibodies against CSP, suggesting the importance of humoral immunity (29, 30). We used IFA (Immunofluorescence assay), which recognizes both stages, to determine the serum reactivity against sporozoites and EEFs (Figure S7).

Discussion

Sporozoites infect liver cells, where they mature into hepatic merozoites that invade red blood cells. Several sporozoite and liver stage-specific proteins have been implicated during liver stage development (5, 10, 31–35). Among them, P36 and P52 are microneme-localized proteins. Disruption of these genes led to growth arrest of the parasite in the liver and yielded GAP. Immunization with GAP parasites elicits immune responses that protect rodents and humans from an infectious sporozoite challenge (Dijk et al., 2005; Kublin et al., 2017; Labaied et al., 2007; A.-K. Mueller et al., 2005; Vaughan et al., 2009). In this study, we investigated the role of a sporozoite and liver stage-specific protein and showed that the expression of Scot1 is similar to the distribution pattern of micronemes. Our analysis of the subcellular localization of Scot1 and TRAP confirmed that Scot1 is a micronemal protein. After establishing the EEF, the micronemes are completely discarded into the PV (3). Parasites lacking the *Plasmodium* autophagy pathway protein Atg7 fail to expel the microneme into the PV (4). We found that Scot1 does not play a role in eliminating

unneeded micronemes during liver stage development. This result indicated that the elimination of micronemes is regulated by the *Plasmodium* autophagy pathway (4) and that microneme-resident proteins are not involved in this process. Several micronemal proteins are involved in the hepatocyte invasion of sporozoites (5, 6, 8), whereas *Scot1* KO sporozoites invade hepatocytes normally, suggesting that Scot1 does not perform multiple essential functions and only plays a role in the development of the EEF. Like P52 and P36 mutants, *Scot1* KO parasites are arrested in the liver. However, compared with early-attenuating P52 and P36 mutants, *Scot1* KO parasites attenuate during late liver stage development (10).

A lack of Scot1 had no effect on blood or mosquito stage development. Scot1 was also found to be dispensable in a *P. falciparum* genetic screen (39). Micronemal proteins have been implicated in the gliding motility and invasion of sporozoites (5, 6, 8). Next, we analysed the invasion ability of *Scot1* KO sporozoites and found it to be normal. Furthermore, the early- to mid-liver-stage development of the *Scot1* KO parasites was normal, and the number and size of the EEFs were comparable to those of the WT GFP. In contrast, *Scot1* deletion affected late liver stage development. Earlier known GAPs, such as UIS3, UIS4 (upregulated in infectious sporozoites) and SPELD mutants, are arrested early before extensive DNA replication (31, 32, 34), while the type II fatty acid synthesis (FASII) pathway and RNA-binding protein *PlasMei2,* liver-stage antigen-1, and liver-specific protein 2 mutants are arrested late in liver stage development (36, 40–43).

The structural superposition with the SCOP and PDB databases using the FATCAT and DALI web services and subsequent superposition of the results in UCSF

Chimera show that the model aligns with the haemoglobin linker chain L1 (chain M of PDB ID 2GTL (red)) with a 0.9 Å RMSD value and chain A of the crystal structure of the vaccine antigen Transferrin Binding Protein B (TbpB) (PDB ID: 4O4X (red)), a metal transport protein with a 0.8 Å RMSD value. The metal transport function prediction of Scot1 suggested that this could be another factor for its phenotype in the liver. The role of metals during liver stage development has been reported previously, and the role of a metal ion transporter, ZIPCO, was found to be critical for EEF development (44). Metals are associated with several processes in mammals and are implicated in oxygen transport in hemoglobin. Iron has been reported to play an essential role in DNA replication as a cofactor for ribonucleotide reductases (45) and metalloproteins. Iron is also essential for DNA replication as a cofactor of ribonucleotide reductases (45) and metalloproteins that contain an iron-sulfur (Fe-S) cluster (46). A study demonstrated that the ZIP protein Leishmania iron transporter 1 is essential for parasite replication in macrophage phagolysosomes (47, 48). The *Scot1* KO phenotype could not be reversed by supplementation with exogenously provided metal ions. A likely explanation for the developmental arrest of Scot1 in the liver stages may be that Scot1 is not a carrier of iron, zinc, or cadmium and can possibly act as a carrier for other small molecules. Another possibility is that Scot1 may detoxify metal/small molecules. In fact, a vacuolar iron transporter (VIT) has been described in *P. berghei* and is involved in detoxifying excess iron (49). Whether Scot1 plays a role in detoxifying excess metal ions requires further investigation.

Immunizations with genetically attenuated sporozoites that arrest in the liver elicit a long-term protective host response (50). We found that vaccination of C57BL/6 mice with *Scot1* KO sporozoites conferred complete protection against WT sporozoite

challenge. Interestingly, late liver-arresting parasites provide superior protection compared to early-arresting parasites (51). Late liver-arresting parasites express late-stage antigens and a subset of antigens that are common to blood stages; however, whether Scot1 GAP exhibits superior protection needs further investigation. Despite the discovery of a growing list of GAPs, there have been some occasional breakthrough infections in a few GAPs. To overcome these limitations, double- or triple-attenuated GAPs can be generated by combination with known late-arresting GAPs (36, 40, 41), which increase the degree of attenuation of these parasites to prevent any possible breakthrough infection. Our investigations demonstrated that Scot1 is essential for late liver-stage development and could be used as a GAP vaccine.

Materials and methods

Parasites and mice

P. berghei ANKA (MRA 311) and *P. berghei* ANKA GFP (MRA 867 507 m6cl1) were obtained from BEI Resources, USA. Swiss albino and C57BL/6 mice were used for parasite infections. All animal procedures were approved by the Institutional Animal Ethics Committee at CSIR-Central Drug Research Institute, India (approval no: IAEC/2018/49).

Amino acid sequence analysis

Interestingly, a study investigating the transcriptional landscape of *Plasmodium vivax* sporozoites revealed several upregulated transcripts with strong orthologues in the sporozoite stages of other species (52). We selected Scot1, which was the top-ranked gene in the transcriptome analysis. The *P. berghei* Scot1

(PBANKA_1411000) sequence was obtained from PlasmoDB (https://plasmodb.org/plasmo/app), and NCBI BLAST (https://blast.ncbi.nlm.nih.gov/Blast.cgi) was used to search for similar sequences in different organisms. Multiple sequence alignment (MSA) was performed using ClustalW. A sequence similarity matrix was prepared using the smith-waterman algorithm implemented in EMBOSS Water (https://www.ebi.ac.uk/jdispatcher/psa/emboss_water). The presence of the signal peptide and transmembrane domain was predicted using SignalP (https://services.healthtech.dtu.dk/services/SignalP-6.0) and TMHMM (https://services.healthtech.dtu.dk/services/TMHMM-2.0/) (53). A phylogenetic tree was constructed using MEGA11 software and the EMBL Interactive Tree Of Life (iTOL) service (https://itol.embl.de) (54).

Generation of transgenic Scot1-3XHA-mCherry parasites to study their expression and localization

For the endogenous tagging of *Scot1* (PBANKA_1411000) with 3XHA-mCherry, two fragments, F1 (0.84 kb) and F2 (0.52 kb), were amplified using primers 1165/1171 and 1167/1168 and cloned into the pBC-3XHA-mCherry-hDHFR vector at *Xho*I/*Bgl*II and *Not*I/*Asc*I, respectively, as previously described (55). The targeting cassette was transfected into *P. berghei* ANKA schizonts (56), clonal lines were obtained by limiting dilution of the parasites, and correct integration was confirmed by diagnostic PCR using primers 1169/1218 and 1215/1170 (Table S2). Next, the mosquito cycle was initiated to observe the expression of mCherry in sporozoites and liver stages as previously described (55).

Generation of *Scot1* knockout and complemented *P. berghei* lines

To delete *Scot*1, two fragments, F3 (0.63 kb) and F4 (0.52 bp), were amplified using the primer sets 1172/1173 and 1167/1168 and cloned into *Sal*I and *Not*I/*Asc*I in the pBC-GFP-hDHFR:yFCU vector. The targeting cassette was transfected into *P. berghei* schizonts, and clonal lines were obtained as described above. Site-specific 5' and 3' integrations were confirmed by diagnostic PCR using primers 2222/1225 and 1215/1170, respectively (Table S2). For complementation, fragment F5 was amplified from *P. berghei* genomic DNA using primers 1172/1168, transfected into *Scot1* KO schizonts, and selected using 5-fluorocytosine (MP Biomedicals, 219979201) as previously described (55). Restoration of the *Scot1* gene was confirmed using primers 1593/1594.

Western blot analysis

Purified sporozoites were resuspended in Laemmli buffer (Bio-Rad, 1610747), analysed by SDS–PAGE and transferred onto nitrocellulose membranes (Bio-Rad, 1620112), and the remaining procedures were performed as previously described (57). Briefly, the membrane was blocked with 1% BSA/PBS, followed by incubation with an anti-mCherry antibody developed in rabbits (diluted 1:500, Novus, NBP 2-25157) and an HRP-conjugated anti-rabbit secondary antibody (Amersham, NA934). The blot was developed using ECL Chemiluminescent Substrate (Bio-Rad, 1705060), and signals were detected using a ChemiDoc XRS+ System (Bio-Rad, USA). As a loading control, the blot was stripped and reprobed with an anti-TRAP antibody (diluted 1:200) (26).

Sporozoite infectivity

To determine the in vivo infectivity of the *Scot1* KO sporozoites, C57BL/6 mice were either intravenously inoculated with salivary gland sporozoites or infected by mosquito bite, and the appearance of the parasite in the blood was observed by performing a Giemsa-stained blood smear. Another group of mice injected with 5,000 sporozoites was sacrificed at 40 and 55 hpi (hours post-infection), and the livers were harvested and homogenized in TRIzol reagent (Invitrogen, USA). To assess the invasion of the *Scot1* KO parasites, HepG2 cells were infected with sporozoites, and the culture was fixed at 1 hpi and immunostained before and after permeabilization with an anti-CSP monoclonal antibody (3D11) (30) as previously described (58). To observe EEF development, HepG2 cells were infected with salivary gland sporozoites and fixed at different time points using 4% paraformaldehyde as previously described (55). For the EEF and detached cell development assays, 5,000 and 40,000 sporozoites/well were added to 48-well and 24-well plates, respectively.

Real-time PCR

Total RNA was isolated using TRIzol reagent, and cDNA was synthesized as previously described (59). The 18S rRNA copy number was determined by absolute quantification of gene-specific standards (60) using primers 1195/1196. The 18S rRNA copy number was normalized to that of mouse glyceraldehyde-3-phosphate dehydrogenase (GAPDH) using primers 1193/1194.

Immunofluorescence assay

For the localization of Scot1 in sporozoites, purified salivary gland sporozoites were allowed to settle and dry on 12-well slides (Thermo Fisher Scientific, USA). Sporozoites were fixed using 4% paraformaldehyde (Sigma–Aldrich, HT5012), permeabilized with 0.1% Triton-X-100 (Sigma–Aldrich, T8787) for 10 min at RT and incubated with anti-mCherry developed in mouse (diluted 1:1000, Biolegend, 677702) and anti-TRAP (diluted 1:200, rabbit polyclonal) (26) antibodies for 2 h at RT. The mCherry and TRAP signals were revealed using Alexa Fluor 594-conjugated anti-mouse IgG and Alexa Fluor 488-conjugated anti-rabbit IgG, respectively (diluted 1:500; Invitrogen). The EEFs fixed at different time points were permeabilized using methanol, blocked using 1% BSA/PBS and incubated with primary antibodies as previously described (57). To visualize the microneme elimination pattern, infected cultures fixed at different time points were immunostained with an anti-TRAP antibody (diluted 1:200) (26). The primary antibodies used were anti-mCherry (diluted 1:500), anti-UIS4 (diluted 1:1,000, rabbit polyclonal) (31), anti-TRAP, anti-MSP1 (diluted 1:5000, mouse monoclonal) (61), and anti-ACP (diluted 1:1,000, rabbit polyclonal) (62). The signals were revealed using Alexa Fluor 488-conjugated or Alexa Fluor 594-conjugated secondary antibodies (diluted 1:500; Invitrogen). Nuclei were stained with Hoechst 33342 (Sigma–Aldrich, 41399), and the coverslips were mounted using Prolong Diamond antifade reagent (Invitrogen, P36970). Representative images were acquired using FV1000 software on a confocal laser scanning microscope (Olympus BX61WI) using UPlanSAPO 100x (NA 1.4, oil) or 63x (NA 0.25, oil).

Bioinformatic analysis of Scot1 proteins

The 3D structure of PfScot1 was predicted using the Quark (https://zhanggroup.org/QUARK) ab initio structure prediction web service. Structure-based phylogenetic analysis was performed using the predicted structure of PfScot1. 3D Phylofold is a recently developed method used to repurpose existing antivirals for COVID-19 treatment (63). The DALI webserver was used to identify structural matches of PfScot1 in the PDB database (64). The top hits from the results were analysed using 3Dphylofold to generate a structure-based similarity matrix. The matrix was further analysed using Mega to generate a nearest-neighbor dendrogram (https://www.megasoftware.net).

Effects of metal supplementation on EEF maturation

HepG2 cells were infected with WT GFP or *Scot1* KO sporozoites as described above. Two hpi, fresh media containing 50 µg /ml ferric ammonium citrate (FAC), 20 µM zinc chloride (ZnCl2) or 1µg/ml cadmium chloride (CdCl2) were added. The media was changed every 12 hours, supplemented with metals. At 65 hpi, culture was observed for the formation of detached cells and then fixed with 4% paraformaldehyde (Sigma–Aldrich, HT5012). The EEFs were stained with an anti-MSP1 antibody, and the nuclei were stained with Hoechst 33342 (Sigma–Aldrich, 41399) as described above. Coverslips were mounted using Prolong Diamond antifade reagent (Invitrogen, P36970). Images were acquired using FV1000 software on a confocal laser scanning microscope (Olympus BX61WI) using UPlanSAPO 100x (NA 1.4, oil) or 63x (NA 0.25, oil).

Immunization and challenge experiments

Six- to eight-week-old female C57BL/6 mice were primed intravenously with 50,000 salivary gland sporozoites and boosted twice with 25,000 at an interval of two weeks. The salivary gland debris of uninfected mosquitoes was injected into the control group. Another group was immunized thrice with 20,000 sporozoites. The control and immunized groups were challenged with 5,000 infectious WT sporozoites 10 days after the last immunization. Parasitemia was monitored daily by making Giemsa-stained blood smears.

Immunized mouse serum reactivity

To visualize the reactivity of sera obtained from the immunized mice, sporozoites and EEFs were stained with pooled serum (diluted 1:50), and signals were revealed using Alexa Fluor 594-conjugated anti-mouse IgG (diluted 1:500; Invitrogen). To identify the sporozoites and EEFs, anti-TRAP (26) and anti-UIS4 antibodies (31), respectively, were used. Nuclei were stained with Hoechst 33342.

Statistical analysis

The data are presented as the mean ± SEM or mean ± SD. Statistical analysis was performed using GraphPad Prism 9 software. As indicated, two-tailed, unpaired Student’s t test and one-way ANOVA were used to determine the statistical significance.

Availability of data and material

All the data are available within this manuscript, and the raw data are available from the corresponding author upon reasonable request. Materials generated in this study are available from the corresponding author upon request.

Acknowledgments

We thank Dr. Robert Menard (Institute Pasteur, France) for the pBC-GFP-hDHFR vector, which was modified by Dr. P.N. Srivastava. We thank Dr. Kota Arun Kumar (University of Hyderabad, India) for the pBC-3XHA-mCherry-hDHFR vector. We thank Dr. Anthony A. Holder (The Francis Crick Institute, UK), Drs. Photini Sinnis and Sean Prigge (Johns Hopkins University, USA) for anti-MSP1, anti-UIS4, and anti-ACP antibodies, respectively. AG, Nirdosh, RD, AM, SKN and PNS were supported by CSIR, UGC ICMR and DBT Research Fellowships. We acknowledge the THUNDER (BSC0102) and MOES (GAP0118) Intravital and Confocal Microscopy Facilities of CSIR-CDRI. The graphics were created with Biorender.com. This work was supported by a Science and Engineering Research Board grant (EMR/2016/006487).

Author contributions

SM conceived the idea, designed the experiments, analysed the data and wrote the manuscript. AG, RD, AM, SKN, N and PNS performed the experiments. All the authors have read and approved the manuscript.

Declaration of interests

The authors declare no competing financial interests.

References

1. World Malaria Report, 2023.
2. LH M, DI B, K M, OK D, Miller LH, Baruch DI, Marsh K, Doumbo OK. 2002. The pathogenic basis of malaria. Nature 415:673–679.
3. Jayabalasingham B, Bano N, Coppens I. 2010. Metamorphosis of the malaria parasite

in the liver is associated with organelle clearance. Cell Res 20:1043–1059.
4. Mishra A, Srivastava PN, H SA, Mishra S. 2023. Autophagy protein Atg7 is essential and druggable for maintaining malaria parasite cellular homeostasis and organelle biogenesis. bioRxiv 2023.08.16.553492.
5. Arredondo SA, Schepis A, Reynolds L, Kappe SHI. 2021. Secretory Organelle Function in the Plasmodium Sporozoite. Trends Parasitol 37:651–663.
6. Sultan AA, Thathy V, Frevert U, Robson KJH, Crisanti A, Nussenzweig V, Nussenzweig RS, Ménard R. 1997. TRAP is necessary for gliding motility and infectivity of plasmodium sporozoites. Cell 90:511–522.
7. Yang ASP, O'Neill MT, Jennison C, Lopaticki S, Allison CC, Armistead JS, Erickson SM, Rogers KL, Ellisdon AM, Whisstock JC, Tweedell RE, Dinglasan RR, Douglas DN, Kneteman NM, Boddey JA. 2017. Cell Traversal Activity Is Important for Plasmodium falciparum Liver Infection in Humanized Mice. Cell Rep 18:3105–3116.
8. Fernandes P, Loubens M, Le Borgne R, Marinach C, Ardin B, Briquet S, Vincensini L, Hamada S, Hoareau-Coudert B, Verbavatz J-M, Weiner A, Silvie O. 2022. The AMA1-RON complex drives Plasmodium sporozoite invasion in the mosquito and mammalian hosts. PLoS Pathog 18:e1010643.
9. Steinbuechel M, Matuschewski K. 2009. Role for the Plasmodium sporozoite-specific transmembrane protein S6 in parasite motility and efficient malaria transmission. Cell Microbiol 11:279–288.
10. Labaied M, Harupa A, Dumpit RF, Coppens I, Mikolajczak SA, Kappe SHI. 2007. Plasmodium yoelii sporozoites with simultaneous deletion of P52 and P36 are completely attenuated and confer sterile immunity against infection. Infect Immun 75:3758–3768.
11. Klug D, Frischknecht F. 2017. Motility precedes egress of malaria parasites from oocysts. Elife 6:1–32.
12. Ecker A, Bushell ESC, Tewari R, Sinden RE. 2008. Reverse genetics screen identifies six proteins important for malaria development in the mosquito. Mol Microbiol 70:209–220.
13. Zavala F. 2022. RTS,S: the first malaria vaccine. J Clin Invest 132.
14. Datoo MS, Natama MH, Somé A, Traoré O, Rouamba T, Bellamy D, Yameogo P, Valia D, Tegneri M, Ouedraogo F, Soma R, Sawadogo S, Sorgho F, Derra K, Rouamba E, Orindi B, Ramos Lopez F, Flaxman A, Cappuccini F, Kailath R, Elias S, Mukhopadhyay E, Noe A, Cairns M, Lawrie A, Roberts R, Valéa I, Sorgho H, Williams N, Glenn G, Fries L, Reimer J, Ewer KJ, Shaligram U, Hill AVS, Tinto H. 2021. Efficacy of a low-dose candidate malaria vaccine, R21 in adjuvant Matrix-M, with seasonal administration to children in Burkina Faso: a randomised controlled trial. Lancet (London, England) 397:1809–1818.
15. Nussenzweig RS, Vanderberg J, Most H, Orton C. 1967. Protective immunity produced by the injection of x-irradiated sporozoites of plasmodium berghei. Nature 216:160–162.
16. Friesen J, Matuschewski K. 2011. Comparative efficacy of pre-erythrocytic whole organism vaccine strategies against the malaria parasite. Vaccine 29:7002–7008.
17. Khan SM, Janse CJ, Kappe SHI, Mikolajczak SA. 2012. Genetic engineering of attenuated malaria parasites for vaccination. Curr Opin Biotechnol 23:908–916.
18. Seder RA, Chang L-JJ, Enama ME, Zephir KL, Sarwar UN, Gordon IJ, Holman LSA, James ER, Billingsley PF, Gunasekera A, Richman A, Chakravarty S, Manoj A, Velmurugan S, Li ML, Ruben AJ, Li T, Eappen AG, Stafford RE, Plummer SH, Hendel CS, Novik L, Costner PJMM, Mendoza FH, Saunders JG, Nason MC, Richardson JH, Murphy J, Davidson SA, Richie TL, Sedegah M, Sutamihardja A,

Fahle GA, Lyke KE, Laurens MB, Roederer M, Tewari K, Epstein JE, Sim BKL, Ledgerwood JE, Graham BS, Hoffman SL. 2013. Protection against malaria by intravenous immunization with a nonreplicating sporozoite vaccine. Science (80-) 341:1359–1365.

19. Epstein JE, Tewari K, Lyke KE, Sim BKL, Billingsley PF, Laurens MB, Gunasekera A, Chakravarty S, James ER, Sedegah M, Richman A, Velmurugan S, Reyes S, Li M, Tucker K, Ahumada A, Ruben AJ, Li T, Stafford R, Eappen AG, Tamminga C, Bennett JW, Ockenhouse CF, Murphy JR, Komisar J, Thomas N, Loyevsky M, Birkett A, Plowe C V, Loucq C, Edelman R, Richie TL, Seder RA, Hoffman SL. 2011. Live attenuated malaria vaccine designed to protect through hepatic $CD8^+$ T cell immunity. Science 334:475–480.
20. Sissoko MS, Healy SA, Katile A, Omaswa F, Zaidi I, Gabriel EE, Kamate B, Samake Y, Guindo MA, Dolo A, Niangaly A, Niaré K, Zeguime A, Sissoko K, Diallo H, Thera I, Ding K, Fay MP, O'Connell EM, Nutman TB, Wong-Madden S, Murshedkar T, Ruben AJ, Li M, Abebe Y, Manoj A, Gunasekera A, Chakravarty S, Sim BKL, Billingsley PF, James ER, Walther M, Richie TL, Hoffman SL, Doumbo O, Duffy PE. 2017. Safety and efficacy of PfSPZ Vaccine against Plasmodium falciparum via direct venous inoculation in healthy malaria-exposed adults in Mali: a randomised, double-blind phase 1 trial. Lancet Infect Dis 17:498–509.
21. Goswami D, Minkah NK, Kappe SHI. 2019. Designer Parasites: Genetically Engineered Plasmodium as Vaccines To Prevent Malaria Infection. J Immunol 202:20–28.
22. Mordmüller B, Surat G, Lagler H, Chakravarty S, Ishizuka AS, Lalremruata A, Gmeiner M, Campo JJ, Esen M, Ruben AJ, Held J, Calle CL, Mengue JB, Gebru T, Ibáñez J, Sulyok M, James ER, Billingsley PF, Natasha KC, Manoj A, Murshedkar T, Gunasekera A, Eappen AG, Li T, Stafford RE, Li M, Felgner PL, Seder RA, Richie TL, Sim BKL, Hoffman SL, Kremsner PG. 2017. Sterile protection against human malaria by chemoattenuated PfSPZ vaccine. Nature 542:445–449.
23. Vaughan AM, Sack BK, Dankwa D, Minkah N, Nguyen T, Cardamone H, Kappe SHII. 2018. A Plasmodium parasite with complete late liver stage arrest protects against preerythrocytic and erythrocytic stage infection in mice. Infect Immun 86:1–18.
24. Manzoni G, Marinach C, Topçu S, Briquet S, Grand M, Tolle M, Gransagne M, Lescar J, Andolina C, Franetich JF, Zeisel MB, Huby T, Rubinstein E, Snounou G, Mazier D, Nosten F, Baumert TF, Silvie O. 2017. Plasmodium P36 determines host cell receptor usage during sporozoite invasion. Elife 6:1–24.
25. Loubens M, Vincensini L, Fernandes P, Briquet S, Marinach C, Silvie O. 2021. Plasmodium sporozoites on the move: Switching from cell traversal to productive invasion of hepatocytes. Mol Microbiol 115:870–881.
26. Mishra A, Varshney A, Mishra S. 2023. Regulation of Atg8 membrane deconjugation by cysteine proteases in the malaria parasite Plasmodium berghei. Cell Mol Life Sci 80:344.
27. Duffy PE. 2022. Current approaches to malaria vaccines. Curr Opin Microbiol 70:102227.
28. Doolan DL, Southwood S, Chesnut R, Appella E, Gomez E, Richards A, Higashimoto YI, Maewal A, Sidney J, Gramzinski RA, Mason C, Koech D, Hoffman SL, Sette A. 2000. HLA-DR-promiscuous T cell epitopes from Plasmodium falciparum pre-erythrocytic-stage antigens restricted by multiple HLA class II alleles. J Immunol 165:1123–1137.
29. Dups JN, Pepper M, Cockburn IA. 2014. Antibody and B cell responses to

673 Plasmodium sporozoites. Front Microbiol 5:625.
674 30. Yoshida N, Nussenzweig RS, Potocnjak P, Nussenzweig V, Aikawa M. 1980.
675 Hybridoma Produces Protective Antibodies Directed against the Sporozoite Stage of
676 Malaria Parasite. Science (80-) 207:71–73.
677 31. Mueller AK, Camargo N, Kaiser K, Andorfer C, Frevert U, Matuschewski K, Kappe
678 SH. 2005. Plasmodium liver stage developmental arrest by depletion of a protein at the
679 parasite-host interface. Proc Natl Acad Sci U S A 102:3022–3027.
680 32. Mueller A-K, Labaied M, Kappe SHI, Matuschewski K. 2005. Genetically modified
681 Plasmodium parasites as a protective experimental malaria vaccine. Nature 433:164–
682 167.
683 33. Aly ASI, Lindner SE, MacKellar DC, Peng X, Kappe SHI. 2011. SAP1 is a critical
684 post-transcriptional regulator of infectivity in malaria parasite sporozoite stages. Mol
685 Microbiol 79:929–939.
686 34. Al-Nihmi FMA, Kolli SK, Reddy SR, Mastan BS, Togiri J, Maruthi M, Gupta R,
687 Sijwali PS, Mishra S, Kumar KA. 2017. A Novel and Conserved Plasmodium
688 Sporozoite Membrane Protein SPELD is Required for Maturation of Exo-erythrocytic
689 Forms. Sci Rep 7:40407.
690 35. van Schaijk BCL, Ploemen IHJ, Annoura T, Vos MW, Foquet L, van Gemert G-J,
691 Chevalley-Maurel S, van de Vegte-Bolmer M, Sajid M, Franetich J-F, Lorthiois A,
692 Leroux-Roels G, Meuleman P, Hermsen CC, Mazier D, Hoffman SL, Janse CJ, Khan
693 SM, Sauerwein RW. 2014. A genetically attenuated malaria vaccine candidate based
694 on P. falciparum b9/slarp gene-deficient sporozoites. Elife 3.
695 36. Vaughan AM, O'Neill MT, Tarun AS, Camargo N, Phuong TM, Aly ASII, Cowman
696 AF, Kappe SHII. 2009. Type II fatty acid synthesis is essential only for malaria
697 parasite late liver stage development. Cell Microbiol 11:506–520.
698 37. Dijk MR Van, Douradinha B, Franke-fayard B, Heussler V, Dooren MW Van, Schaijk
699 B Van, Gemert G Van, Sauerwein RW, Mota MM, Waters AP, Janse CJ. 2005.
700 Genetically attenuated , P36p-deficient malarial sporozoites induce protective
701 immunity and apoptosis of infected liver cells 102.
702 38. Kublin JG, Mikolajczak SA, Sack BK, Fishbaugher ME, Seilie A, Shelton L,
703 VonGoedert T, Firat M, Magee S, Fritzen E, Betz W, Kain HS, Dankwa DA, Steel
704 RWJJ, Vaughan AM, Sather DN, Murphy SC, Kappe SHII, Noah Sather D, Murphy
705 SC, Kappe SHII. 2017. Complete attenuation of genetically engineered Plasmodium
706 falciparum sporozoites in human subjects. Sci Transl Med 9:1–12.
707 39. Zhang M, Wang C, Otto TD, Oberstaller J, Liao X, Adapa SR, Udenze K, Bronner IF,
708 Casandra D, Mayho M, Brown J, Li S, Swanson J, Rayner JC, Jiang RHYY, Adams
709 JH. 2018. Uncovering the essential genes of the human malaria parasite Plasmodium
710 falciparum by saturation mutagenesis. Science (80-) 360.
711 40. Yu M, Kumar TRS, Nkrumah LJ, Coppi A, Retzlaff S, Li CD, Kelly BJ, Moura PA,
712 Lakshmanan V, Freundlich JS, Valderramos J-C, Vilcheze C, Siedner M, Tsai JH-C,
713 Falkard B, Sidhu ABS, Purcell LA, Gratraud P, Kremer L, Waters AP, Schiehser G,
714 Jacobus DP, Janse CJ, Ager A, Jacobs WRJ, Sacchettini JC, Heussler V, Sinnis P,
715 Fidock DA. 2008. The fatty acid biosynthesis enzyme FabI plays a key role in the
716 development of liver-stage malarial parasites. Cell Host Microbe 4:567–578.
717 41. Dankwa DA, Davis MJ, Kappe SHI, Vaughan AM. 2016. A Plasmodium yoelii Mei2-
718 like RNA binding protein is essential for completion of liver stage schizogony. Infect
719 Immun 84:1336–1345.
720 42. Mikolajczak SA, Sacci JB, De La Vega P, Camargo N, Vanbuskirk K, Krzych U, Cao
721 J, Jacobs-Lorena M, Cowman AF, Kappe SHI. 2011. Disruption of the plasmodium
722 falciparum liver-stage antigen-1 locus causes a differentiation defect in late liver-stage

parasites. Cell Microbiol 13:1250–1260.
43. Orito Y, Ishino T, Iwanaga S, Kaneko I, Kato T, Menard R, Chinzei Y, Yuda M. 2013. Liver-specific protein 2: A Plasmodium protein exported to the hepatocyte cytoplasm and required for merozoite formation. Mol Microbiol 87:66–79.
44. Sahu T, Boisson B, Lacroix C, Bischoff E, Richier Q, Formaglio P, Thiberge S, Dobrescu I, Ménard R, Baldacci P. 2014. ZIPCO, a putative metal ion transporter, is crucial for Plasmodium liver-stage development. EMBO Mol Med 6:1387–1397.
45. Sanvisens N, Bañó MC, Huang M, Puig S. 2011. Regulation of ribonucleotide reductase in response to iron deficiency. Mol Cell 44:759–769.
46. Wu Y, Brosh RMJ. 2012. DNA helicase and helicase-nuclease enzymes with a conserved iron-sulfur cluster. Nucleic Acids Res 40:4247–4260.
47. Huynh C, Sacks DL, Andrews NW. 2006. A Leishmania amazonensis ZIP family iron transporter is essential for parasite replication within macrophage phagolysosomes. J Exp Med 203:2363–2375.
48. Huynh C, Andrews NW. 2008. Iron acquisition within host cells and the pathogenicity of Leishmania. Cell Microbiol 10:293–300.
49. Slavic K, Krishna S, Lahree A, Bouyer G, Hanson KK, Vera I, Pittman JK, Staines HM, Mota MM. 2016. A vacuolar iron-transporter homologue acts as a detoxifier in Plasmodium. Nat Commun 7:1–10.
50. Overstreet MG, Cockburn IA, Chen YC, Zavala F. 2008. Protective CD8+ T cells against Plasmodium liver stages: Immunobiology of an “unnatural” immune response. Immunol Rev 225:272–283.
51. Butler NS, Schmidt NW, Vaughan AM, Aly AS, Kappe SHII, Harty JT. 2011. Superior antimalarial immunity after vaccination with late liver stage-arresting genetically attenuated parasites. Cell Host Microbe 9:451–462.
52. Westenberger SJ, McClean CM, Chattopadhyay R, Dharia N V., Carlton JM, Barnwell JW, Collins WE, Hoffman SL, Zhou Y, Vinetz JM, Winzeler EA. 2010. A systems-based analysis of Plasmodium vivax lifecycle transcription from human to mosquito. PLoS Negl Trop Dis 4.
53. Sonnhammer EL, von Heijne G, Krogh A. 1998. A hidden Markov model for predicting transmembrane helices in protein sequences. Proceedings Int Conf Intell Syst Mol Biol 6:175–182.
54. Letunic I, Bork P. 2016. Interactive tree of life (iTOL) v3: an online tool for the display and annotation of phylogenetic and other trees. Nucleic Acids Res 44:W242-5.
55. Srivastava PN, Mishra S. 2022. Disrupting a Plasmodium berghei putative phospholipase impairs efficient egress of merosomes. Int J Parasitol 52:547–558.
56. Janse CJ, Ramesar J, Waters AP. 2006. High-efficiency transfection and drug selection of genetically transformed blood stages of the rodent malaria parasite Plasmodium berghei. Nat Protoc 1:346–356.
57. Narwal SK, Nayak B, Mehra P, Mishra S. 2022. Protein kinase 9 is not required for completion of the Plasmodium berghei life cycle. Microbiol Res 260:127051.
58. Rénia L, Miltgen F, Charoenvit Y, Ponnudurai T, Verhave JP, Collins WE, Mazier D. 1988. Malaria sporozoite penetration A new approach by double staining. J Immunol Methods 112:201–205.
59. Choudhary HH, Gupta R, Mishra S. 2019. PKAc is not required for the preerythrocytic stages of Plasmodium berghei 2:1–11.
60. Bruña-Romero O, Hafalla JC, González-Aseguinolaza G, Sano G, Tsuji M, Zavala F. 2001. Detection of malaria liver-stages in mice infected through the bite of a single Anopheles mosquito using a highly sensitive real-time PCR. Int J Parasitol 31:1499–

1502.
61. Holder AA, Freeman RR. 1981. Immunization against blood-stage rodent malaria using purified parasite antigens. Nature 294:361–364.
62. Gallagher JR, Prigge ST. 2010. Plasmodium falciparum acyl carrier protein crystal structures in disulfide-linked and reduced states and their prevalence during blood stage growth. Proteins 78:575–588.
63. Sun YJ, Velez G, Parsons DE, Li K, Ortiz ME, Sharma S, McCray PBJ, Bassuk AG, Mahajan VB. 2021. Structure-based phylogeny identifies avoralstat as a TMPRSS2 inhibitor that prevents SARS-CoV-2 infection in mice. J Clin Invest 131.
64. Holm L. 2022. Dali server: structural unification of protein families. Nucleic Acids Res 50:W210–W215.

807 **Table 1.** Infectivity of salivary gland sporozoites in C57BL/6 mice. Blood smears were
808 examined daily from day 3 onwards, and the mice were considered negative if
809 parasites were not detected by day 20. NA, not applicable.

810

Experiments	Parasites	Sporozoites inoculated	Mice positive/mice inoculated	Prepatent period (day)
1	WT	5,000	10/10	3
	Scot1 KO	5,000	0/15	NA
	Scot1 comp	5,000	5/5	3
	WT	Via 20 mosquitos bite	5/5	3
	Scot1 KO	Via 20 mosquitos bite	0/5	NA
2	WT	10,000	10/10	3
	Scot1 KO	10,000	0/20	NA
	Scot1 comp	5,000	5/5	3
3	WT	50,000	5/5	3
	Scot1 KO	50,000	0/10	NA

811
812
813
814
815
816
817
818
819
820
821
822
823
824
825
826
827
828
829
830
831
832
833
834
835
836
837

838 **Table 2.** Infectivity of the merosomes in Swiss mice. Blood smears were examined
839 daily from day 1 onwards, and the mice were considered negative if parasites were not
840 detected by day 20. NA, not applicable.

841

Experiment	Parasite	Number of detached cells injected	Mice positive/mice inoculated	Prepatent period (day
1	WT	10	5/5	2.4
	Scot1 KO	Supernatant	0/5	NA
2	WT	100	5/5	1.2
	Scot1 KO	Supernatant	0/5	NA

842
843
844
845
846
847
848
849
850
851
852
853
854
855
856
857
858
859
860

Table 3. Infectivity of the merosomes in Swiss mice. Metal ion supplementation did not affect the *Scot1* KO phenotype. Blood smears were examined daily from day 1 onwards, and the mice were considered negative if parasites were not detected by day 20. NA, not applicable.

Parasite	Number of detached cells injected	Mice positive/mice inoculated	Prepatent period (day)
WT	10	10/10	2.5
WT+ FAC	10	10/10	2.6
WT+ ZnCl2	10	10/10	2.7
WT+ CdCl2	10	10/10	2.7
Scot1 KO	Supernatant	0/10	NA
Scot1 KO + FAC	Supernatant	0/10	NA
Scot1 KO + ZnCl2	Supernatant	0/10	NA
Scot1 KO + CdCl2	Supernatant	0/10	NA

894 **Table 4. Immunization of C57BL/6 mice with *Scot1*-KO sporozoites protects**
895 **against infection.** Mice were immunized with the indicated number of *Scot1* KO
896 sporozoites and challenged on day 10 after the last immunization with *P. berghei* WT
897 sporozoites. All immunized mice were protected from WT *P. berghei* sporozoite
898 challenge. NA, not applicable.

899

Experiment	Group	Immunization dose	Challenge day	Challenge dose	No. of patent/no. of challenged	Prepatent period (day)
1	Control	(3x) SG debris	10	5,000	5/5	3
	Scot1 KO	1x) $5x10^4$ and (2x) $2.5x10^4$	10	5,000	0/5	NA
2	Control	(3x) SG debris	10	5,000	5/5	3
	Scot1 KO	1x) $5x10^4$ and (2x) $2.5x10^4$	10	5,000	0/5	NA
3	Control	(3x) SG debris	10	5,000	5/5	3
	Scot1 KO	(3x) $2x10^4$	10	5,000	0/5	NA

900
901
902
903
904
905
906
907
908
909
910
911
912
913

Figure legends

Figure 1. Expression and localization of Scot1 in *P. berghei*. (A) Scot1-3XHA-mCherry salivary gland sporozoites showing mCherry expression pattern. **(B)** HepG2 cells infected with Scot1-3XHA-mCherry sporozoites were harvested at different time points. Cultures harvested at 12, 24, 36, 48, and 62 hpi were stained with mCherry and UIS4 antibodies, and nuclei were stained with Hoechst. mCherry expression was observed at 12, 24, and 62 hpi but at 36 and 48 hpi. **(C)** Confirmation of the expression of the Scot1 fusion protein in the Scott1-3XHA-mCherry transgenic parasites using an anti-mCherry antibody. A 39 kDa band was detected in the lysate of the Scot1 transgenic sporozoites but not in the lysate of the WT parasites. The blot was stripped and reprobed with an anti-TRAP antibody as a loading control. **(D)** IFA of Scot1-3XHA-mCherry transgenic sporozoites using anti-TRAP and anti-mCherry antibodies. TRAP and mCherry were colocalized (PCC=0.9 of 10 sporozoites).

Figure 2. *Scot1* KO parasites exhibit major defects during late liver stage development. (**A**) To quantify the parasite burden, infected mouse livers were harvested at 40 and 55 hpi, RNA was isolated, and transcripts were quantified using real-time PCR. The *P. berghei* 18S rRNA copy number was comparable in the WT GFP and *Scot*1 KO parasites at 40 hpi (P=0.5233, Student's t test) but decreased in the *Scot*1 KO parasites compared to the WT GFP parasites at 55 hpi (*P=0.0248, Student's t test). The data are presented as the means ± SDs; n = 5 mice per group.

Figure 3. *Scot1* KO EEFs exhibit normal growth but fail to mature into hepatic merozoites. (A) HepG2 cells infected with the *Scot*1 KO or WT GFP sporozoites

were harvested at different time points. Cultures harvested at 24, 36, 48, and 62 hpi were stained with anti-UIS4 antibody, and host and parasite nuclei were stained with Hoechst. The EEFs grew normally until 48 hpi and showed impaired nuclear division at 62 hpi. **(B)** The number of EEFs in the *Scot1* KO parasites at 36 (P=0.1426), 48 (P=0.7006) and 62 hpi (P=0.2518) was not significantly different from that in the WT GFP. The data were obtained from three independent experiments performed in duplicate and are presented as the mean ± SEM. **(C)** The EEF area at 36 (P=0.2064), 48 (P=0.2084) and 62 hpi (P=0.0908) was comparable between the WT GFP and *Scot1* KO parasites. The data were obtained from three independent experiments performed in duplicate and are presented as the mean ± SEM. **(D)** The number of EEFs from the *Scot1* KO and WT GFP parasites. Despite a comparable number of EEFs, *Scot1* KO parasites failed to release detached cells into the culture supernatant (***P<0.0003). The data were obtained from a single experiment performed in duplicate and are presented as the mean ± SD. Student's t test was used to determine the statistical significance.

Figure 4. *Scot1* KO EEFs exhibit impaired late liver stage development. (A) Culture fixed at 62 hpi was immunostained with the apicoplast marker anti-ACP antibody. WT GFP and *Scot1* KO parasites showing apicoplast branching patterns. (**A**) Infected cultures harvested at 62 hpi were immunostained with an anti-MSP1 antibody to visualize the development of hepatic merozoites, and DNA was stained with Hoechst. No merozoites were observed in the *Scot1* KO parasites. We found normal segregation of nuclei and the formation of merozoites in the WT GFP parasites but not in the *Scot1* KO parasites. **(B)** Nuclei were counted in WT GFP, *Scot1* KO and Scot1 comp EEFs at 62 hpi, and a significant decrease in nuclear

965 count was observed in *Scot1* KO parasites (****P<0.0001, Student's t test). No
966 significant difference was observed between WT GFP and Scot1 comp parasites (P=
967 0.5166, Student's t test).
968
969 **Figure 5. The *Scot1* KO parasites expel micronemes normally.** HepG2 cultures
970 infected with the *Scot1* KO or WT GFP parasites were fixed at 24, 40, and 55 hpi
971 and immunostained with anti-TRAP antibodies. During the liver stage of *Plasmodium*
972 development, micronemes were expelled into the PV in both the *Scot1* KO and WT
973 GFP parasites. Nuclei were stained with Hoechst.
974
975 **Figure 6. Bioinformatic analysis indicated that Scot1 is a metal/small molecule**
976 **carrier protein.** (**A**) The structure of PfScot1, as predicted using the Quark ab initio
977 structure prediction web service, shows an open beta-barrel configuration. **(B)**
978 Superposition of PfScot1 (gold) with chain M of PDB ID 2GTL (red) with a 0.9 Å
979 RMSD value and **(C)** chain A of PDB ID 4O4X (red) with a 0.8 Å RMSD value. **(D)**
980 Structure-based phylogenetic tree depicting the relative position of PfScot1
981 (highlighted) among its closest matching PDB counterparts listed in Table S1.
982
983 **Figure 7. Metal ion supplementation does not rescue the *Scot1* KO phenotype**.
984 HepG2 cells were infected with either *Scot1* KO or WT GFP sporozoites and cultured
985 in media supplemented with different concentrations of metal ions. The culture was
986 observed at 65 hpi for the formation of detached cells and then fixed for IFA. (**A**) No
987 detached cells were observed in the *Scot1* KO parasites supplemented with metal
988 ions (****P<0.0001, one-way ANOVA). (**B**) Merozoites were not observed in the
989 *Scot1* KO parasites supplemented with metal ions (***P= 0.0002, one-way ANOVA).

(**C**) Impaired nuclear division in *Scot1* KO parasites supplemented with metal ions (****P<0.0001, one-way ANOVA). The data were obtained from two independent experiments performed in duplicate and are presented as the mean ± SEM.

Supplemental Material

Figure S1. Phylogenetic tree.

Figure S2. Scot1 amino acid sequence analysis.

Figure S3. Generation of Scot1-3XHA-mCherry parasites and their development in the mosquito and liver stages.

Figure S4. Generation of *Scot1* KO and complemented parasites.

Figure S5. The development of *Scot1* KO parasites in mosquitoes.

Figure S6. *Scot1* KO sporozoites invade hepatocytes normally.

Figure S7. Immune sera recognize sporozoites and the EEF.

Table S1. Closest structure-based phylogenetic matches of PfSCOT1 from the PDB database.

Table S2. List of primers used in this study.

Figure 1

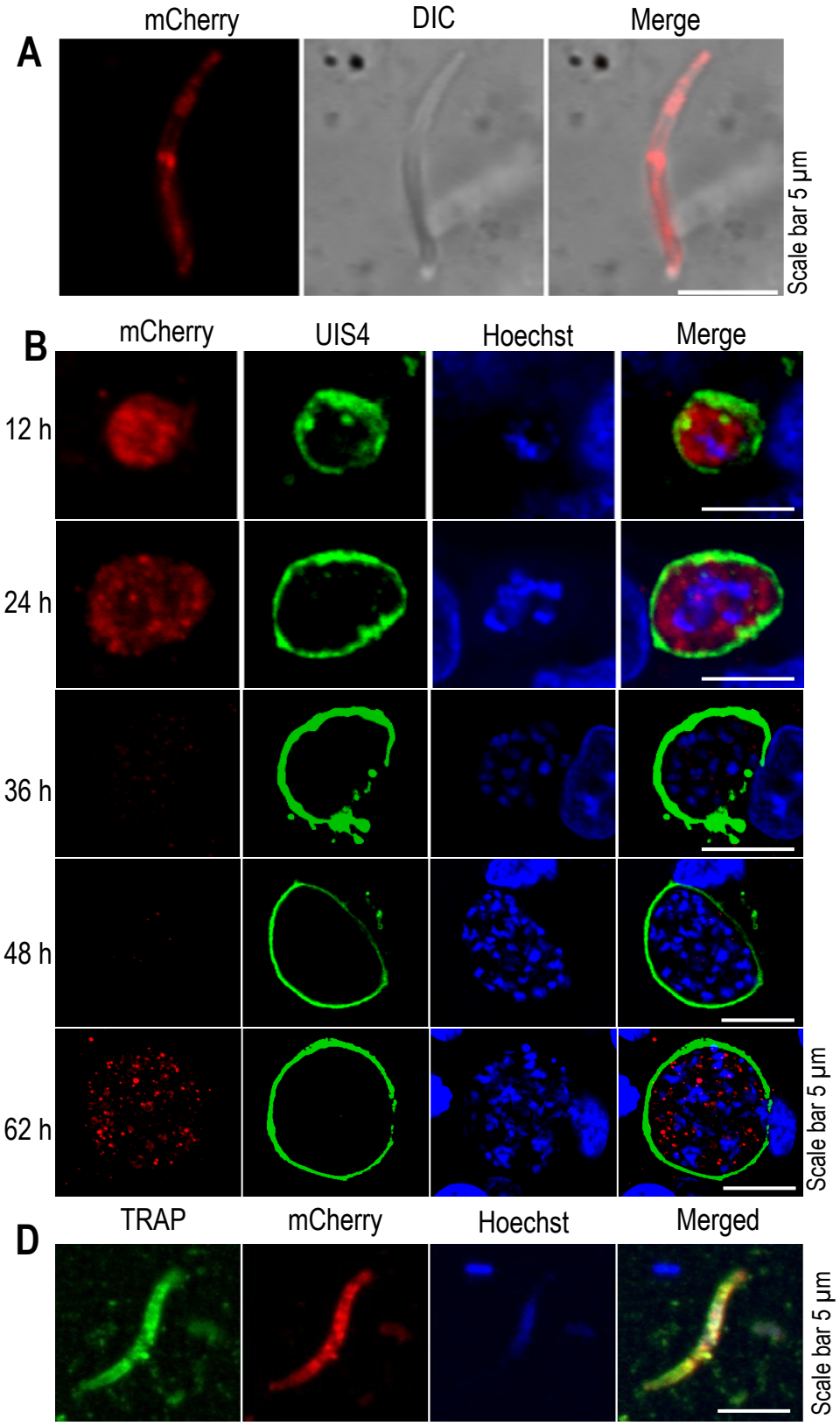

Figure 2

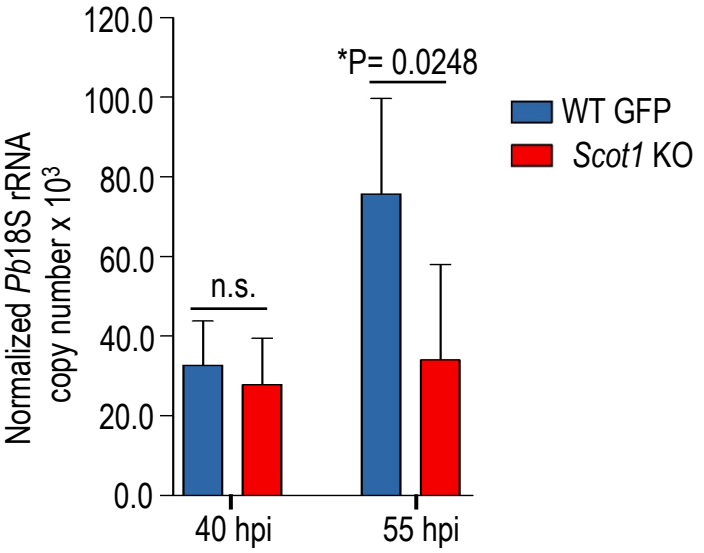

Figure 3

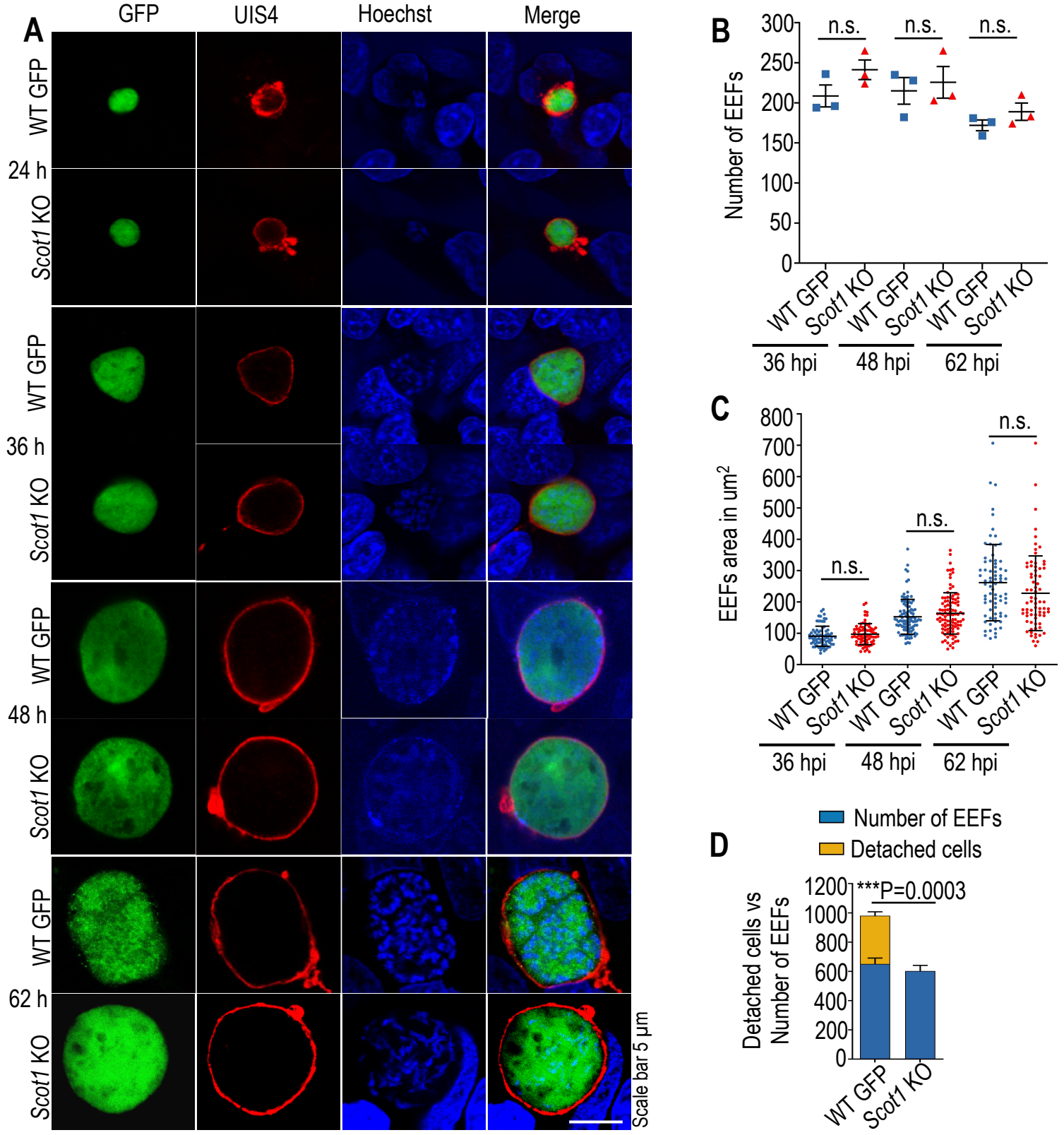

Figure 4

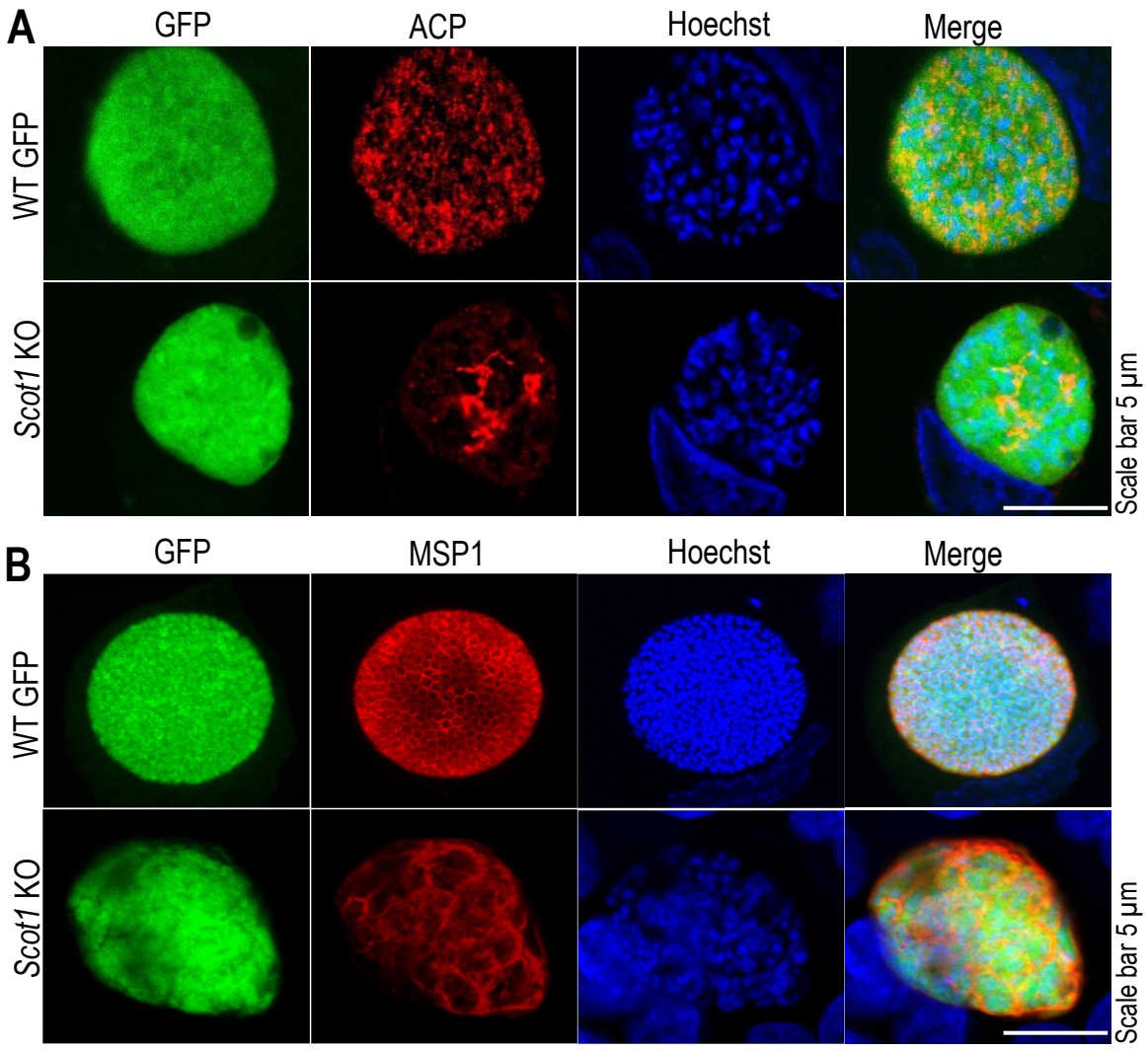

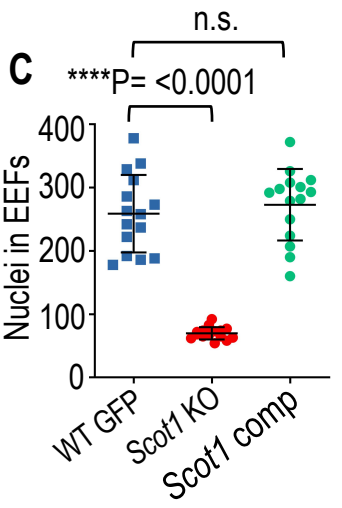

Figure 5

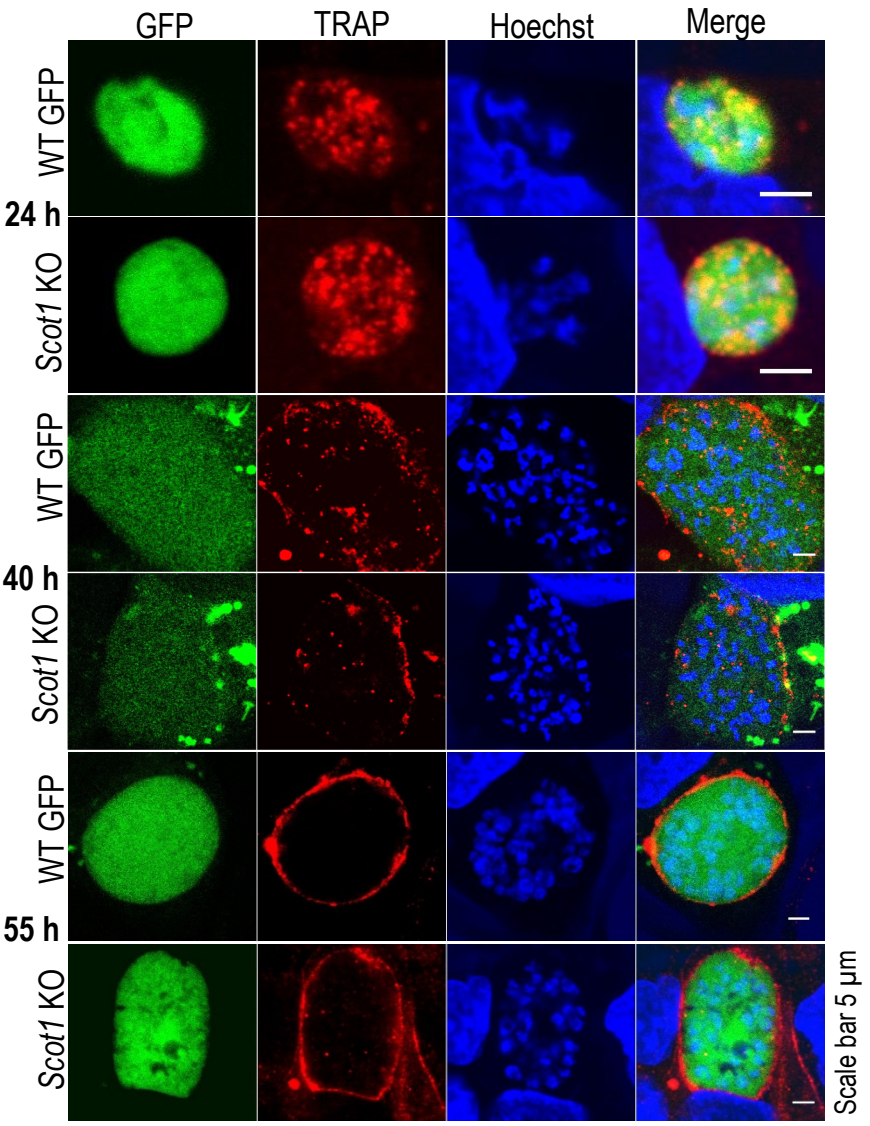

Figure 6

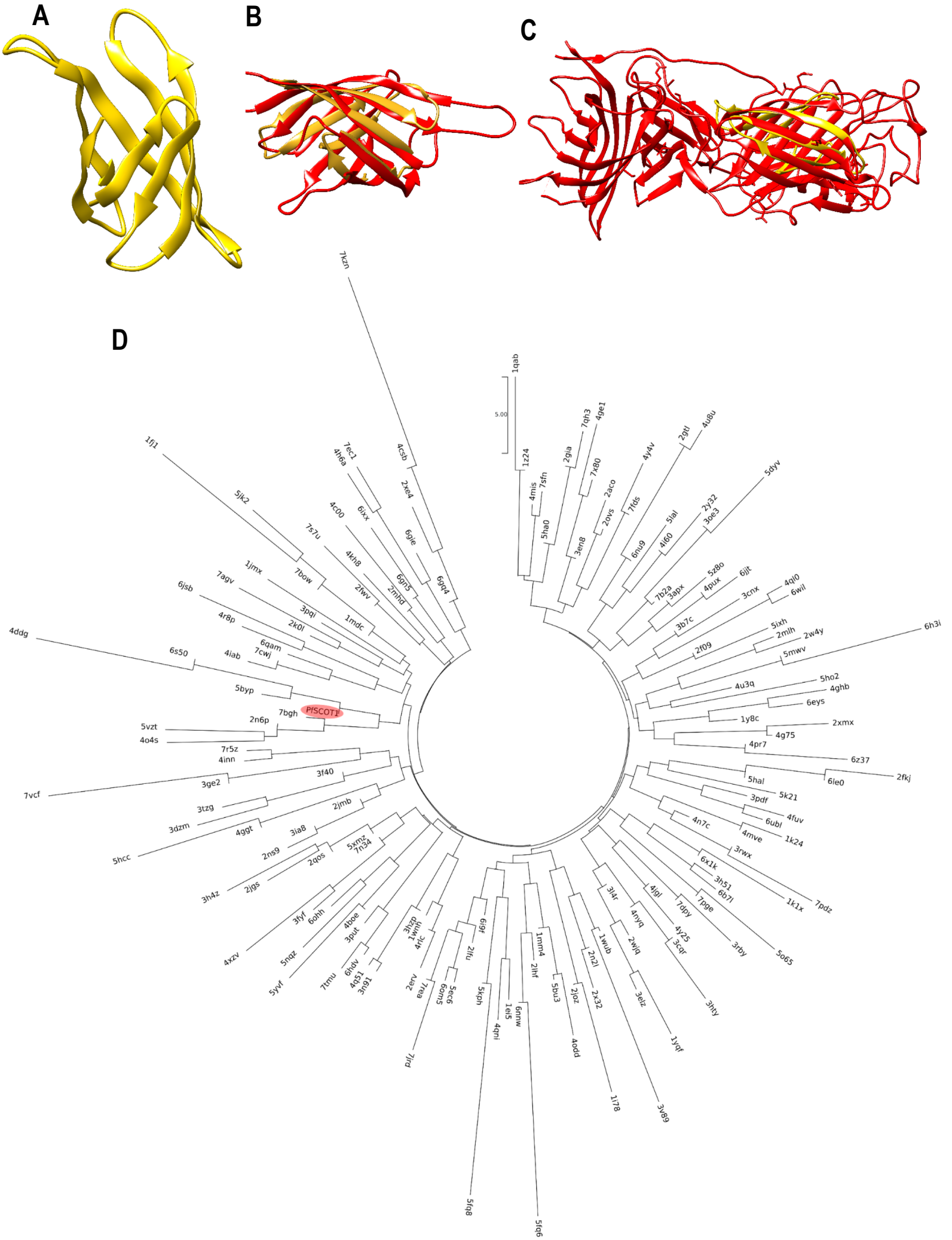

Figure 7